EXPERIMENTAL STUDY OF HYDRODYNAMIC PARAMETERS REGARDING ON GEYSER BOILING PHENOMENON IN GLASS THERMOSYPHON USING WIRE-MESH SENSOR

by

Diogenes OLIVEIRA DE SOUZA[a], Pedro Leineker OCHOSKI MACHADO[b], Conrado CHIARELLO[a], Eduardo NUNES DOS SANTOS[a], Marco Jose DA SILVA[a], Paulo Henrique DIAS DOS SANTOS[a], and Thiago ANTONINI ALVES [b*]

[a] Multiphase Flow Center (NUEM), Federal University of Technology – Parana, Curitiba, Brazil
[a] Federal University of Technology – Parana, Ponta Grossa, Brasil

Original scientific paper
https://doi.org/10.2298/TSCI201008221O

The thermosyphon is a type of heat exchanger that has been widely used in many applications. The use of thermosyphons has been intensified in recent years, mainly in the manufacture of solar collectors and various industrial activities. A thermosyphon is a vertical sealed tube filled with a working fluid, consisting of, from bottom to top, by an evaporator, an adiabatic section, and a condenser. The study of geyser-boiling phenomena, which occurs inside the thermosyphon is of extreme importance, therefore the experimental analysis of the parameters related to the two-phase flow (liquid-steam), such as void fraction, bubble frequency, bubble velocity, and bubble length are necessary, since these parameters have a significant influence on heat transfer. In this work, a pair of wire mesh sensors was used, a relative innovative technology to obtain experimental values of the reported quantities for measuring these parameters of slug flow in thermosyphons. An experimental set-up is assembled and the sensors are coupled to the thermosyphon enabling the development of the experimental procedure. Here is presented an experimental study of a glass thermosyphon instrumented with two wire-mesh sensors, in which the aforementioned slug flow hydrodynamic parameters inherent to the geyser type boiling process are measured. It was measured successfully, as a function of the heat load (110, 120, 130, 140, and 150 W), the void fraction (instantly and average), liquid film thickness, translation velocity of the elongated bubbles, lengths of the bubbles, and the liquid slug (displaced by the bubble rise up). It was observed that the higher the heat load, the lower is the bubble translation velocity. For all heat loads, based on the measured length of liquid slug (consequent displacement of liquid volume), caused by bubbles rise from evaporator to condenser, it could be affirmed to some extent that both boiling regime (pool and film) exist in the evaporator. The measured average void fraction (80%) and liquid film thickness (around 2.5 mm) during the elongated bubble passages were approximately constant and independent of the heat load.

Key words: *glass thermosyphon, geyser boiling, hydrodynamic parameters, slug flow, wire-mesh sensor*

* Corresponding author, e-mail: antonini@utfpr.edu.br

Introduction

Thermosyphons are heat pipes that do not have a porous or capillary structure to move the working fluid inside of them [1]. Gravitational action is the driving force that causes the working fluid to move, therefore the condenser must always be above the evaporator. [2]. Thermosyphons are devices that transfer heat with high performance and have a broad range of applications in engineering [3]. In particular, they are widely used in solar heating systems, both in industry and for heating domestic water [4-6].

Geyser-type boiling is an unstable phenomenon occurring within the thermosyphons. When elongated bubbles are generated in the evaporator, they expand rapidly and hatch in the region of the condenser causing characteristic vibrations and sounds. A pioneering work published by Griffith [7] presented a study of this type of boiling phenomena in thermosyphons. The geyser phenomenon occurs when a determined confined working fluid is in the liquid state and is heated. The liquid becomes superheated (metastable state) and suddenly changes to the vapor state, forming large bubbles that coalesce into an elongate bubble that grows and moves upwards abruptly, striking the condenser region. This phenomenon occurs periodically in the boiling process in thermosyphons for high filling ratios.

The mechanisms of geyser-boiling phenomena in a thermosyphon were investigated by Kuncoro *et al.* [8]. The authors analyzed it experimentally through measurements of temperature and pressure, and by visualization of the phenomenon in a 2.5 m long glass thermosyphon. A schematic diagram of the geyser phenomenon is presented based on visualizations. Even though an explanation of the main thermodynamics' causes is given, the authors did not regard the hydrodynamic characteristics of the phenomenon.

Specifically in the geyser phenomenon occurring for high filling ratios, the hydrodynamic characteristics of the slug flow – such as bubble translation velocity, bubble lengths, and bubble frequencies – are not usually measured experimentally. However, for churn flow [9] has already developed a subatmospheric boiling study regarding geysering instability of a thermosyphon using wire-mesh sensor (WMS) data. These parameters are of paramount importance for the development of a mathematical model capable of estimating the heat transfer coefficient by boiling of the geyser type.

In this context, this work presents an experimental study of a glass thermosyphon instrumented with two WMS, in which the aforementioned slug flow hydrodynamic parameters inherent to the geyser type boiling process are measured. It was measured successfully, as a function of the heat load (110, 120, 130, 140, and 150 W), the void fraction (instantly and average), liquid film thickness, translation velocity of the elongated bubbles and length of liquid slug displaced by the bubble rise up.

Experiment

Thermosyphons, in general, have three distinct regions: evaporator, adiabatic section, and condenser [10]. In the evaporator, the heat is transferred from an external source to working fluid, which boils, and the steam rises afterward [11]. The adiabatic section is the section in which two-phase flow is observed. The present study places WMS where the adiabatic region theoretically exists. Finally, the condenser is the region where heat is transferred from the vapor to the environment. The water vapor condenses and returns by the action of gravity to the evaporator, ending the thermodynamic cycle [12]. The steps of the process can be seen in fig. 1.

The experimental set-up, fig. 2, was assembled in the facilities of the Multiphase Flow Center (NUEM/UTFPR/Curitiba/Brazil) to study the parameters related to the liquid-gas two-phase slug flow found during the geyser boiling process inside the thermosyphon. A glass thermosyphon with an internal diameter of 25.4 mm and an external diameter of 30 mm with a total length of 875 mm is assembled together with the appropriately coupled WMS. The evaporator has a length of 320 mm and the condenser has a length of 475 mm. The region where WMS are installed has a length of 80 mm. The working fluid is water. Tests are performed for a 100% filling ratio to simulate the geyser phenomenon.

The evaporator region was heated using a ribbon resistor (nickel-chromium alloy). The electrical resistor was connected directly to a power source to provide various heat transfer rates applied to the evaporator and heat the working fluid, achieving boiling. Temperatures along the thermosyphon were measured using *T*-type thermocouples attached to the outer surface of the evaporator, the insulation, and the condenser. One of the thermocouples was used to measure the ambient temperature. Two platinum thermoresistors (RTD PT100) were used to measure the internal vapor temperature, while two pressure transducers (Omega Engineering PX419), which measure absolute pressure up to 50 psi (344.7 kPa), were used to measure the internal pressure at two points within the evaporator. The information collected through the thermocouples, thermoresistors, and pressure transducers is analyzed in a computer that receives this information through a data acquisition system (Agilent 34970A).

Figure 3 shows the holes that give access to the inner side of the glass tube, equipped with sensors for data acquisition of temperature and internal pressure of the working fluid. It is also shown the ribbon resistor with 0.1 mm of thickness and 3.5 mm of width that was used to heat the evaporator by the Joule effect created by power dissipation.

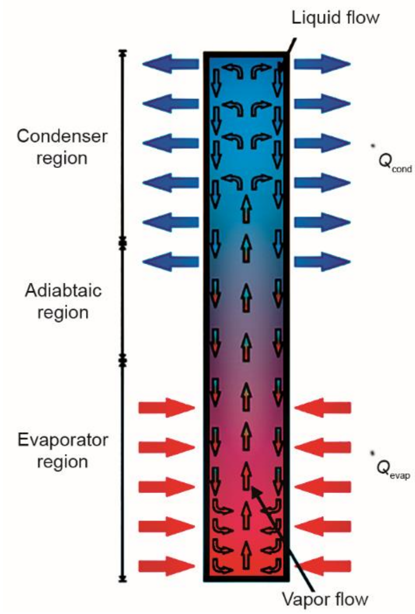

Figure 1. Sketch of thermosyphon operation system [12]

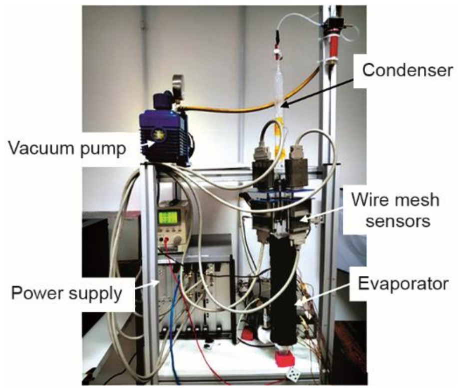

Figure 2. Experimental set-up

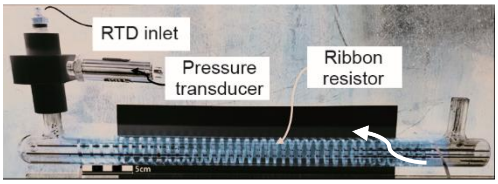

Figure 3. Details of the ribbon resistor assembly and the holes for installing the thermoresistor in the evaporator

All sensors were calibrated and the experimental uncertainties were estimated based on [13]. The uncertainty of the thermocouples, thermoresistors, and pressure transducer was estimated to be ±0.1 °C, ±0.05 °C, and ±2 psi (13.8 kPa), respectively. The experimental uncertainty of WMS readings for void fraction was 5% according to [14], and the expanded uncertainty of translation bubble velocity and length of the liquid slug was up ±6.24%.

Wire-mesh sensors

The electronic capacitive mesh sensor (WMS) is a device that can reconstruct images at high spatial and temporal resolutions by measuring signals relative to two-phase flow, and is accepted as an alternative technique for tomographic imaging of multiphase flow [15, 16]. The associated electronics measure the electrical property (*e.g.*, capacitance) in the gaps of all crossing points that are then converted into phase fraction distributions [14]. Such sensors have been successfully used by several researchers to investigate different phenomena related to two-phase flow, including in two-phase flow in thermosyphons for churn flow by [9].

The sensor consists of two sets of stainless steel wires tensioned over the cross-section with an axial spacing of a few millimeters and at an orthogonal angle to each other, thus forming a grid of electrodes. One electrode is the transmitter, while the other is the receiver. Also, the images generated by the wire mesh sensor are processed to obtain relevant two-phase flow parameters [17]. Figure 4(a) shows a schematic diagram of the resistive mesh sensors and fig. 4(b) shows details of the crossover between the receivers and transmitters.

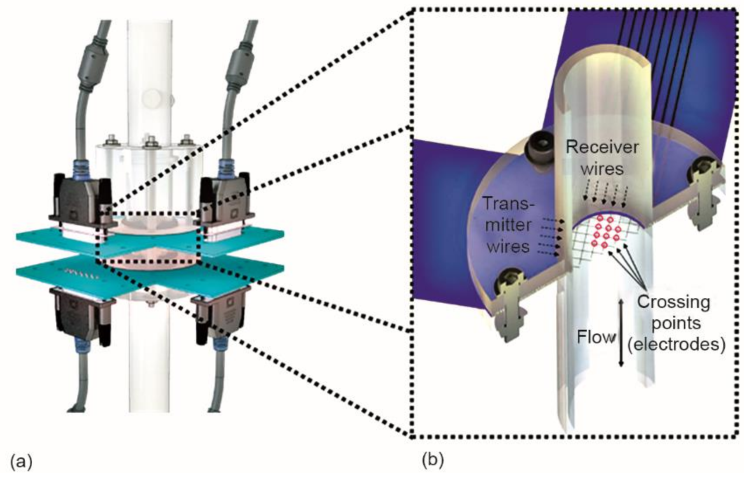

Figure 4. (a) Installation of the sensors and (b) details of the receivers and transmitters

Two 8 × 8 capacitive loop sensors (8 receivers and 8 transmitters) were used in this work. The receiver electrodes are excited and the transmitter response depends on the electrical capacitance of the fluid flowing through the wire mesh. The acquisition frequency was fixed at 400 fps. The electrical capacitance can be expressed as a linear function of the permittivity at the measuring point. In other words, it is assigned a value of 0 when the sensor is traversed only by water and 1 when it is traversed only by the vapor phase. Therefore, to perform the measurements, a reference calibration was required for the tube filled with water to obtain the reference value of void fraction equal to zero.

To obtain the void fraction distributions, a calibration routine is performed with water only, being assigned for this situation $\alpha(i, j, k) = 0$, and with steam only, assigning the value $\alpha(i, j, k) = 1$. The resulting 3-D matrix for the void fraction corresponds to:

$$\alpha(i,j,k)=\frac{V_{\mathrm{H}}(i,j)-V_{\mathrm{L}}(i,j,k)}{V_{\mathrm{H}}(i,j)-V_{\mathrm{L}}(i,j)} \tag{1}$$

where i and j represent the spatial positions and k the time variable, V_{L} – the lowest value of electrical permittivity (air), and V_{H} – the highest value of electrical permittivity (water). To analyze the results, sequences of void fractions, as well as cross section images of the thermosyphon, can be generated. Integrating these data in space and/or time one can obtain the average void fraction $\alpha(k)$:

$$\alpha(k)=\sum_i\sum_j a_{i,j}\,\alpha(i,j,k) \tag{2}$$

where $a_{i,j}$ is the contribution of each intersection point (i, j) to the total cross-sectional area.

In a region that corresponds to the end of the evaporator length, two WMS were installed, responsible for detecting the bubble flow parameters. Details of the sensor assembly in the thermosyphon are shown in fig. 5 for a better understanding of the results obtained.

Figure 5 shows the assembly of the sensors in a region where the adiabatic region would theoretically be. The distance between the two sensors, 26 mm, can also be seen. This distance must be known to determine the translation speed of the bubble.

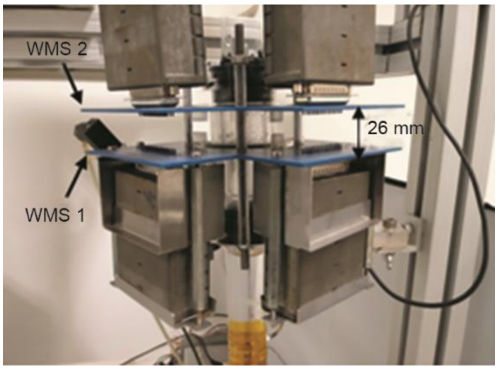

Figure 5. Details of the experimental set-up of the capacitive mesh sensors

Through the information obtained with the WMS, it was possible to determine the parameters of the two-phase flow such as void fraction, bubble translation speed, bubble frequency, and length of the liquid piston displaced by the elongated bubble (will be explained in the sequence). The procedure was performed for heat transfer rates of 110, 120, 130, 140, and 150 W.

Results and discussion

Before presenting the results, it is necessary to schematically explain the phenomenon that will be presented through the data obtained. Figure 6 presents a schematic picture of the evaporator section up to the region where the two WMS are located. In fig. 6(a) the heating of the evaporator is shown: the working fluid (water), in the liquid phase, is heated by heat transfer and, at first, the natural convection process occurs. When the water reaches its saturation temperature, small bubbles begin to appear on the internal surfaces of the tube, fig. 6(b).

These small bubbles detach themselves from the inner walls and rise until they reach the free surface of the liquid-vapor interface, which is approximately at the boundary of the evaporator. Only a few ripples appear at this interface due to the upward movement of the bubbles. As the evaporator continues to be heated, these small bubbles coalesce and form a large elongated bubble, fig. 6(c), which has a diameter close to the pipe diameter and causes a piston of liquid to be propelled from the evaporator into the condenser region (which is not shown in fig. 6).

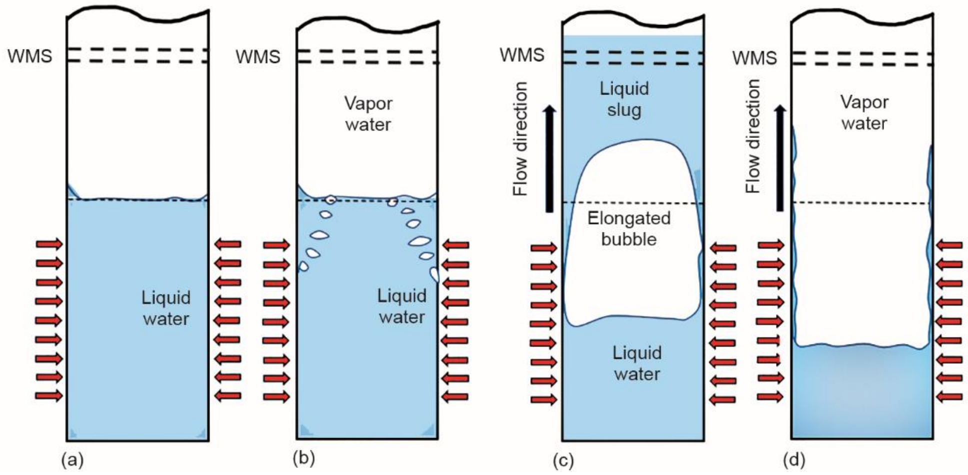

Figure 6. Schematic diagram of the boiling phenomenon in the thermosiphon; (a) heating of the working fluid, (b) formation of small bubbles, (c) liquid piston and elongated bubble moving towards the condenser, and (d) formation of a region with stagnant liquid and a region with a liquid film

In this way, the evaporator is divided into two parts: the upper part with a film of liquid formed between the elongated bubble, and the lower part with liquid with small bubble generation. These two phenomena are called film boiling (upper part) and pool boiling (lower part), fig. 6(d). The phenomenon of large elongated bubbles appearing lasts for seconds and then ceases. The liquid returns to the phenomenon shown in fig. 6(b), forming small bubbles that after a few seconds coalesce instantaneously (almost explosively), forming the elongated bubbles that move very quickly to the condenser region, characterizing the geyser phenomenon.

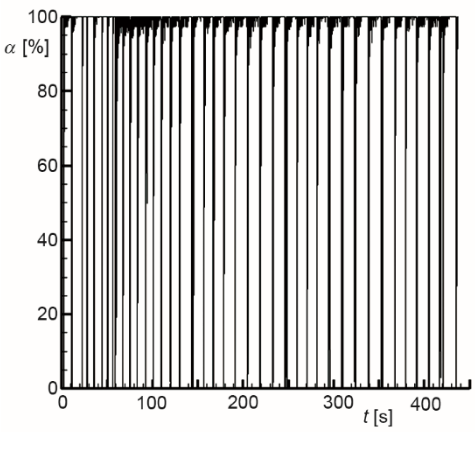

Figure 7. Signal obtained for the vacuum fraction for 150 W heat rate

The main parameter that is measured using the WMS in the glass thermosyphon is the average void fraction of the boiling phenomenon in space, $\bar{\alpha}(t)$. The data were obtained for a time interval of approximately 436 seconds (7.26 minutes) for each heat transfer rate applied. The measured signal for $\bar{\alpha}(t)$ at the WMS 1 sensor over time is shown in fig. 7 for the heat rate of 150 W.

In fig. 7, the intermittent character of the slug flow inside the evaporator can be seen. Each peak corresponds to an elongated bubble that passes through the sensor. When the $\bar{\alpha}(t)$ value is 100% it means that only water vapor is passing through, and when the $\bar{\alpha}(t)$ value is 0% it means that only water is passing through. When the value of $\bar{\alpha}(t)$ was between these two values, an elongated bubble, a countercurrent liquid film flow with the elongated bubble, and a chaotic wake region with many dispersed bubbles were intermittently observed.

Before starting the void fraction measurement, it was ensured that the boiling process was occurring according to the measured temperature and pressure data, fig. 8. Figure 8(a) shows the temperature variation as a function of time for the thermocouple along the outer surface of the evaporator, T_{evap}, the outer surface of the condenser, T_{cond}, and the outer surface of the insulation, T_{insul}, at the 150 W heat rate. When a heat rate is applied to the evaporator, the temperatures of the evaporator thermocouples, T_{evap}, start to rise. Part of this energy is transferred to the working fluid, causing it to heat up (sensible heat) until a plateau is reached at which boiling begins. Note that the saturation temperature, T_{sat}, (thermoresistor installed inside the thermosyphon, just above the evaporator) of the system also begins to increase. The temperature rise is abrupt at about 500 seconds. The saturation temperature, T_{sat}, increases until a maximum peak of approximately 96.5 °C is reached, in which a drop in evaporator temperatures is observed. At this condition, the boiling process begins.

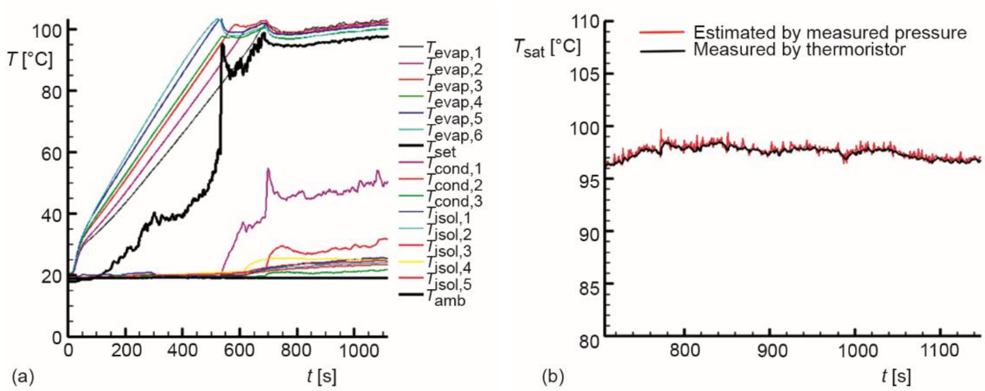

Figure 8. Temperature variation as a function of time for the 150 W heat rate measured by; (a) thermocouples along the thermosyphon on the external surface and (b) by the thermoresistor and calculated as a function of the internal pressure *(for color image see journal web site)*

Figure 8(b) shows the saturation temperature variations measured by the RTD PT100 thermoresistor – which was inserted in the thermosyphon – and estimated indirectly (using the ENGINEERING EQUATION SOLVER software) as a function of the internal pressure measured by the pressure transducer. The time interval is the period during which boiling occurs. Since the temperatures measured by the thermoresistor have a good agreement (maximum deviation of 1.56%) with the saturation temperature estimated using the pressure measured by the pressure transducer, the temperatures measured using the thermoresistor were adopted as the saturation temperature of the vapor during the boiling process.

Once it is assured that boiling is occurring, a breakdown of the signal for a 25 seconds time slot (taken from fig. 6), ranging from the time instant of 150-175 seconds, is presented in fig. 9 for a better explanation of the phenomena captured by the WMS.

Initially, bubbles with diameters much smaller than the internal diameter of the thermosyphon start to form and detach from the internal surface. At this early stage, only water vapor is passing through the WMS 1 sensor and the $\bar{\alpha}(t)$ measured is 100%. It should be noted here that the water in the liquid state lies just below the WMS 1 sensor, so as long as the elongated bubble does not form and rise with sufficient energy, pushing the column of liquid ahead of it, only the vapor phase is detected. As the boiling process progresses, these small

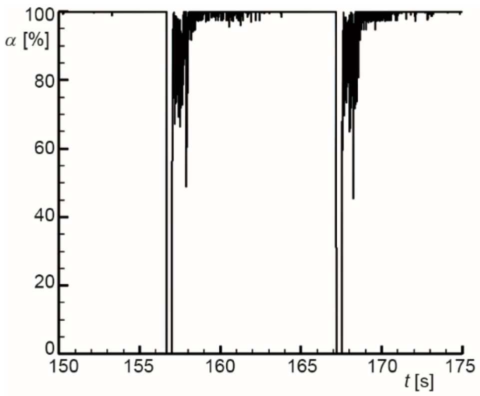

Figure 9. Void fraction for a heat rate of 150 W and a time slot of 25 seconds

bubbles start to coalesce into an elongated bubble that, as it rises by thrust from the bottom of the evaporator to the condenser, displaces the liquid column above it (liquid piston). Figure 9 shows the occurrence of this phenomenon through the measured signal, which is equal to 0%, in the time interval between 156-157 seconds. Note that after a time interval the phenomenon repeats itself with a new elongated bubble crossing the WMS 1 sensor between 167-168 seconds, emphasizing the intermittent nature of the slug flow.

The signal $\bar{\alpha}(t)$ is in good agreement with the actual images obtained with the high-speed camera for the boiling phenomenon, fig. 10. In figure 10(a) the boiling phenomenon is occurring with only water vapor. Then the liquid piston starts to be displaced, fig. 10(b), and then only liquid starts to pass through the WMS 1 sensor, fig. 10(c). Finally, the elongated bubble that caused the displacement of the liquid piston appears, fig. 10(d).

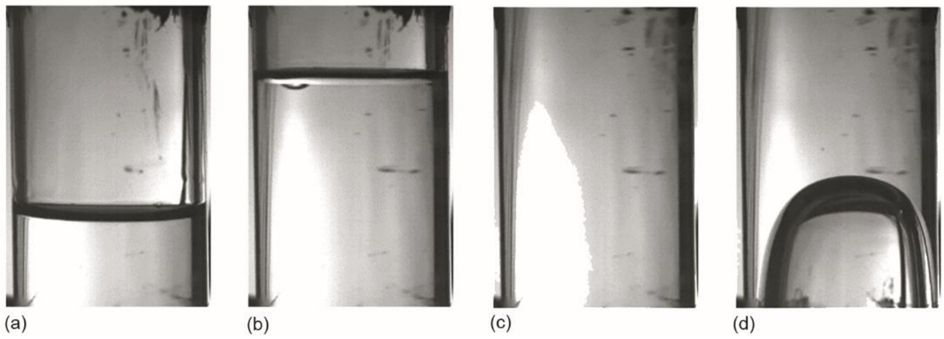

Figure 10. Liquid piston passing through the WMS; (a)-(c) displacement of the liquid column, and (d) passage of the elongated bubble

In fig. 10(d) the sensor begins to capture the water vapor signal that corresponds to the front of the elongated bubble. This bubble passes through the sensor causing the signal $\bar{\alpha}(t)$ that was indicating 0, *i.e.* only liquid was passing through the sensor, to start indicating the increase in the percentage of void fraction, as indicated in fig. 11(a). The occurrence of the phenomenon is very fast, the void fraction goes from 0% to almost 100% in the time interval between 157.0-157.2 seconds. As the bubble rises towards the condenser, a liquid film forms between the elongated bubble and the inner surface of the thermosyphon (red dotted line in fig. 11(b). This film is formed by the liquid that flows together with the bubble and the condensate that descends from the condenser by the action of gravity. In the end, the elongated bubble collapses, forming a turbulent wake that is shown in fig. 11(c).

To perform the bubble translation velocity, U_T, analysis, the time interval captured by the sensors for the tip (or nose) of the bubble is measured. Figure 12 shows the detail measured by sensors WMS 1 and WMS 2 when an elongated bubble passes by them in a time interval between 156.8-157.4 seconds for a heat rate of 150 W.

From figure 12 is possible to observe two different signals referring to the passage of a bubble through the sensors. There is a sudden increase of the signal $\bar{\alpha}(t)$ detected by the

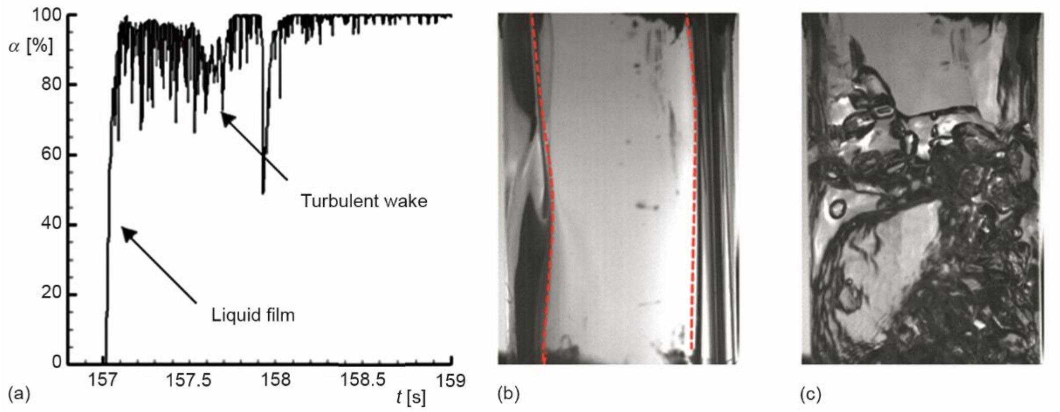

Figure 11. (a) Signal of the void fraction related to the bubble passage, (b) liquid film, and (c) bubble mat *(for color image see journal web site)*

WMS 1, represented by the color in black, exemplifying that the bubble nose is passing by the first sensor. Then, after approximately 10 ms (0.01 second), there is a sudden increase of the detected WMS 2 signal, represented by the color in red. Using this data it is possible to measure the time interval for the detection of the bubble front as it passes by each sensor. Since the distance between the two sensors is known (26 mm), as shown in fig. 4, the bubble velocity is estimated using:

$$U_{\mathrm{T}} = \frac{L_{\mathrm{WMS}}}{\Delta t_B} \tag{3}$$

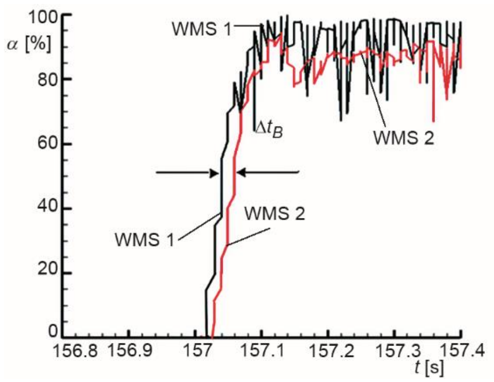

Figure 12. Time lag between the arival of the bubble at the two sensors

The values estimated using eq. (3) are presented in tab. 1 for each heat rate applied to the evaporator for the three tests performed and the average value between them. Note that as the evaporator power increases, the bubble translation speed decreases.

Table 1. Mean values for the bubble translational velocity, U_{T}

Test	Heat rate				
	110 W	120 W	130 W	140 W	150 W
#1	1.41 m/s	1.29 m/s	1.17 m/s	1.08 m/s	1.06 m/s
#2	1.42 m/s	1.20 m/s	1.12 m/s	1.06 m/s	1.03 m/s
#3	1.44 m/s	1.18 m/s	1.07 m/s	1.09 m/s	0.99 m/s
Average	1.42 m/s	1.22 m/s	1.12 m/s	1.07 m/s	1.03 m/s

It was observed that when the lower heat rate was applied, the boiling phenomenon took longer to start. That is, the working fluid in the liquid state received energy until it reached its saturation condition and remained in the liquid state longer. Probably the working fluid entered a metastable equilibrium and did not change phase, even though it was in the saturated condition. Suddenly small bubbles began to coalesce and form an elongated bubble, which explosively rose by thrust, pushing a liquid piston from the evaporator region to the condenser region. This displacement of the liquid piston and the elongated bubble lasted for tenths of a second.

Therefore, what was observed was that the longer the working fluid was heated and remained in its saturated condition, without the formation of the elongated bubble, the higher was the velocity of formation and translation of the bubble. That is, the working fluid entered its metastable state and continued to receive energy without changing phase and somehow this energy was explosively converted into the driving force that caused the bubble formation and translation to occur. This phenomenon is known as the geyser phenomenon.

For the 110 W heat rate, the working fluid was heated and remained in its saturated condition for approximately 20 minutes until the first elongated bubble appeared and the geyser process began. For the 120 W heat rate, this phenomenon took approximately 17 minutes to start. For 130 W approximately 15.7 minutes, for 140 W approximately 15.1 minute, and finally for 150 W, it took approximately 14.5 minutes. For this reason, the bubble translation speed for the 110 W heat rate was the highest among the measured rates due to the longer time it received energy and remained in its saturation state without changing phase (metastable state).

A probability density function is shown in fig. 13, emphasizing the frequency of occurrence of the bubbles according to the translation speed. It can be seen from this figure that for a heat rate of 110 W the average bubble speed is around 1.4 m/s. This result is corroborated with the information provided in tab. 1.

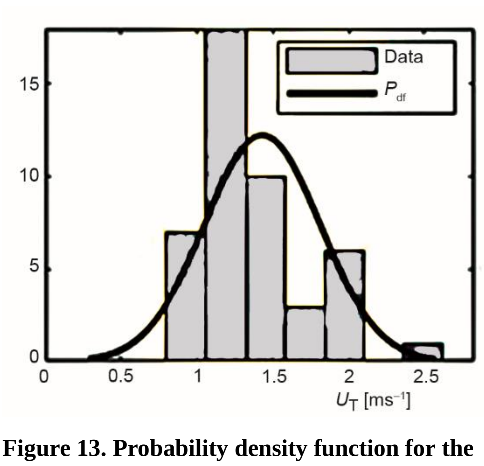

Figure 13. Probability density function for the speed measurements (110 W)

Through a computational routine implemented in the MATLAB software, a two-dimensional reconstruction of the bubble can be made for the best visualization of the phenomenon. Figure 14 shows a 2-D reconstruction of an elongated bubble for each WMS. This simulation was performed based on the variation of the void fraction of the spatial and time series obtained from the WMS.

The lag between the signals, fig. 14(a), allows the determination of the time interval between the passage of the bubble in sensor WMS 1 and sensor WMS 2. The same phenomenon is observed in fig. 14(b) in sensor WMS 2. In figure 14(c), it is initially observed that sensor WMS 1 detects only the presence of liquid since the void fraction is equal to 0%. When the elongated bubble passes through the sensor the signal reaches almost 100%, which evidences the passage of the elongated bubble through the sensor. The time-averaged void fraction was obtained for the unit cell shown in fig. 14 and the results are presented in tab. 2.

The results show some agreement between the void fractions obtained for the indicated heat rates. As always, an elongated bubble was formed, regardless of the applied rate, whose diameter was apparently in the dimension of the internal diameter of the thermosyphon. The average void fraction was very similar and the liquid film thickness, δ_f, was estimated, as shown schematically in fig. 15, ranging between 2.45 mm and 2.56 mm.

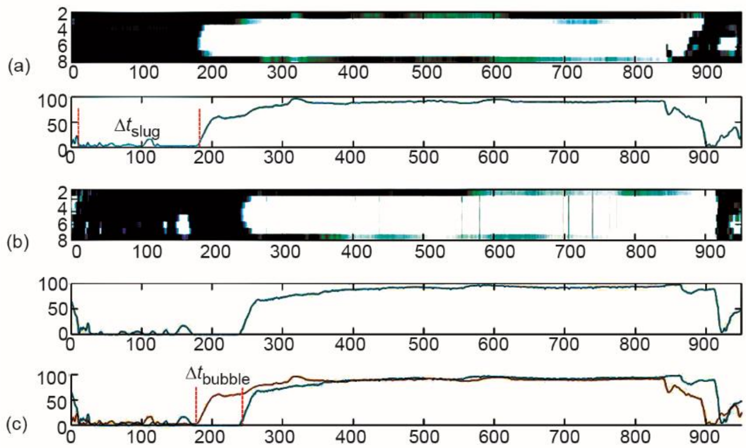

Figure 14. Bubble reconstruction with the aid of the WMS and the MATLAB software; (a) signal lag, (b) image of the bubble in WMS 1, and (c) image of the bubble in WMS 2

Table 2. Void fraction mean values, *α*

Test	Heat rate				
	110 W	120 W	130 W	140 W	150 W
#1	81.59%	81.06%	82.67%	81.18%	79.72%
#2	81.72%	78.90%	78.76%	79.44%	82.02%
#3	78.35%	80.87%	79.22%	80.08%	77.86%
Average	80.55%	80.28%	80.72%	80.56%	79.86%

In fig. 16, a probability density curve is shown for the results obtained in tab. 2. Note that the average of the values obtained for the void fraction shown in this figure corresponds to approximately 80% and is in agreement with the values shown in tab. 2.

Another parameter analyzed was the liquid piston length ahead of the bubble, as shown in fig. 14(a). The liquid column (piston) is pushed vertically upwards due to the formation of elongated bubbles inside the evaporator. At the start of the boiling process, small bubbles form on the inner surface of the glass wall of the evaporator, and over time these bubbles coalesce to form large pockets of vapor (elongated bubble) that rise to the condenser, pushing together the liquid that is above the region where the elongated bubble is formed. To determine this liquid piston flowing in front of the elongated bubble, it was assumed that the translation speed of the liquid piston was the same as the translation speed of the elongated bubble (estimated from the WMS data). With this, it was possible to determine the length of the liquid piston using:

$$L_S = U_T \Delta t_{\text{piston}} \tag{4}$$

where L_s is the length of the liquid column, the dark region in front of the bubble that is shown in fig. 14(a) and Δt_{piston} – the time that the liquid passes through sensor WMS 1. The results obtained for the heat rates according to eq. (4) are shown in tab. 3.

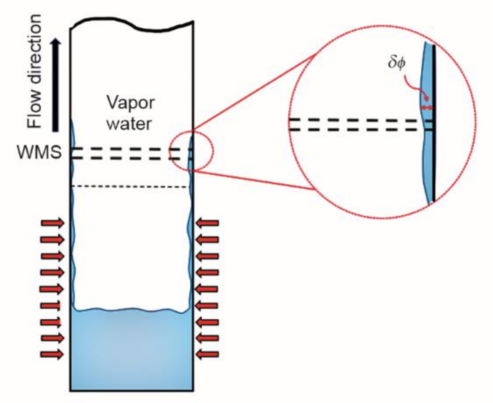

Figure 15. Schematic diagram for estimating the liquid film thickness

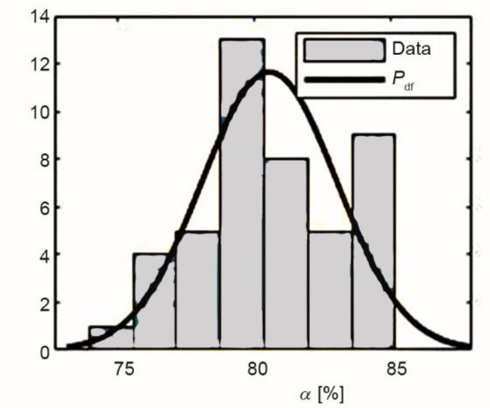

Figure 16. Probability density function for the void fraction measurements (110 W)

Table 3. Mean values for piston length, L_s, pool boiling length, $L_{\text{pool boiling}}$, and piston passage time, Δt_{piston}

Parameter	Heat rate				
	110 W	120 W	130 W	140 W	150 W
Δt_{piston}	0.098 s	0.132 s	0.157 s	0.172 s	0.186 s
L_S	13.86 m	16.08 m	17.60 m	18.43 m	19.13 m
$L_{pool\ boiling}$	18.14 cm	15.92 cm	14.40 cm	13.57 cm	12.87 cm

Table 3 shows the mean values obtained experimentally for the length of the liquid piston that is displaced due to the bubble movement. As a consequence of the displacement of this liquid piston, occurs an emptying in the evaporator region and the length of liquid remaining at the bottom of the thermosyphon can be calculated. As there is no driving force that causes this liquid to remain in the lower part of the thermosyphon to rise, it can be stated that pool boiling occurs in this region, and the length of this region, $L_{\text{pool boiling}}$, was also calculated for each heat rate.

It can be seen that the higher the heat rate applied, the greater the fluid displacement through the elongated bubble and the lower the fluid volume that remains in the evaporator. Therefore, it can be stated that the higher the heat rate, the greater the region in which film boiling occurs and the smaller the region in which pool boiling occurs.

Conclusion

In the present study, an experimental bench was developed to obtain hydrodynamic parameters of the slug flow of the geyser phenomenon inherent to the boiling process in the evaporator of a glass thermosyphon using WMS, temperature, and pressure sensors, and a high-speed camera. This data should be used in future validations of theoretical results obtained from numerical models, and elucidate boiling heat transfer phenomena. The working fluid used was water for a fill ratio of 100%. The heat transfer rates supplied to the evaporator were 110, 120, 130, 140, and 150 W.

The measured average void fraction varied from 79.86% (150 W) up to 80.55% (110 W) and liquid film thickness varied from 2.45 mm (110 W) and 2.56 mm (150 W), thus these two parameters were approximately constant during the elongated bubble passages and they were approximately independent of the heat loads. It was also observed for 150 W that the average translation velocity of the bubble was 1.30 m/s and for 110 W it was 1.42 m/s. That is, the higher the heat load, the lower is the bubble translation velocity. This non-proportionality of the bubble translation speed can be explained because, for the lower heat rates, the boiling phenomenon took longer to start. As an example, for the 110 W rate, the working fluid was heated and remained in its saturated condition for approximately 20 minutes until the first elongated bubble appeared and the geyser process started. For 150 W it took approximately 14.5 minutes. For this reason, the bubble translation speed for the 110 W heat rate was the highest among the measured rates due to the longer time it received power and remained in its saturated state without changing phase (metastable state).

Finally, it was observed that when the bubbles rise from evaporator to condenser, a liquid slug was generated in front of the bubbles. These lengths of liquid slug were measured and varied from 13.86 cm (110 W) up to 19.13 cm (150 W). Thus, there was a consequent displacement of liquid volume from the evaporator to the condenser and the lengths of liquid that remained in the evaporator were estimated and varied from 18.14 cm (110 W) up to 12.87 cm (150 W). Consequently, it could be affirmed, to some extent, that occurs film boiling at the upper part of the evaporator and pool boiling at the bottom of the evaporator.

References

[1] Krambeck, L., *et al*., Experimental Thermal Performance of Different Capillary Structures for Heat Pipes, *Energy Engineering (Print)*, *118* (2021), 1, pp. 1-14
[2] Santos, P. H. D., *et al*., E., Analysis of a Flat Capillary Evaporator with a Bi-Layered Porous Wick, *Thermal Science*, *24* (2020), 3B, pp. 1951-1962
[3] Krambeck, L., *et al*., Thermal Performance Evaluation of Different Passive Devices for Electronic Cooling, *Thermal Science*, *23* (2019), 2B, pp. 1151-1160
[4] Jafari, D., *et al*., Two-Phase Closed Thermosyphons: A Review of Studies and Solar Applications, *Renewable and Sustainable Energy Reviews*, *53* (2016), Jan., pp. 575-593
[5] Poulad, M. E., Fung, A., Potential Benefits from Thermosyphon-PCM (TP) Integrated Design for Buildings Applications in Toronto, *Proceedings*, The Canadian Conference on Building Simulation, Halifax, Canada, 2012, pp. 601-614
[6] Machado, P. L. O., *et al.*, Thermal Performance of Thermosyphons Intended for Evacuated Tube Solar Collector Using Graphene Oxide Nanofluids, *Journal of Nature, Science & Technology*, *1* (2021), 1, pp. 14-19
[7] Griffith, P., Geysering in Liquid-Filled Lines, *Proceedings*, ASME-AICHE Heat Transfer Conference and Exhibit, Houston, Tex., USA, 1962
[8] Kuncoro H., *et al.*, An Experimental Study on the Mechanism of Geysering in a Closed Two-Phase Thermosyphon, *International Journal of Multiphase Flow*, *21* (1995), 6, pp. 1243-1252
[9] Agunlejika, E. O., *et al*., Subatmospheric Boiling Study of the Operation of a Horizontal Thermosyphon Reboiler Loop: Instability, *Applied Thermal Engineering*, *109* (2016), A, pp. 739-745

[10] Nishida, F. B., *et al*., Experimental Investigation of Heat Pipe Thermal Performance with Microgrooves Fabricated by Wire Electrical Discharge Machining (Wire-EDM), *Thermal Science*, *24* (2020), 2A, pp. 701-711
[11] Krambeck, L., *et al*., Experimental Research of Capillary Structure Technologies for Heat Pipes, *Acta Scientiarum Technology (online)*, *42* (2020), 1, e48189
[12] Santos, P. H. D., *et al*., Modeling and Experimental Tests of a Copper Thermosyphon, *Acta Scientiarum Technology (online)*, *39* (2017), 1, pp. 59-68
[13] ***, Evaluation of measurement data, Guide to the Expression of Uncertainty in Measurement, Joint Committee for Guides in Metrology-JCGM 100, 2008 (ISO/IEC Guide 98-3), *http://www.iso.org/sites/JCGM/GUM-introduction.htm*
[14] Silva, M. J. D., *et al.*, Capacitance Wire-Mesh Sensor for Fast Measurement of Phase Fraction Distributions, *Measurement Science and Technology*, *18* (2007), 7, pp. 2245-2251
[15] Prasser, H.-M., *et al*., A New Electrode-Mesh Tomograph For Gas-Liquid Flows, *Flow Measurement and Instrumentation*, *9* (1998), 2, pp. 111-119
[16] Kesana, N. R., *et al.*, Visualization of Gas-Liquid Multiphase Pseudo-Slug Flow using Wire-Mesh Sensor, *Journal of Natural Gas Science and Engineering*, *46* (2017), Oct., pp. 477-490
[17] Furuya, M., *et al*., Three-Dimensional Velocity Vector Determination Algorithm for Individual Bubble Identified with Wire-Mesh Sensors, *Nuclear Engineering and Design*, *336* (2017), Sept., pp. 74-79

Paper submitted: October 8, 2020
Paper revised: April 8, 2021
Paper accepted: April 16, 2021